Journal of Materials Chemistry C

ROYAL SOCIETY OF CHEMISTRY

COMMUNICATION

View Article Online
View Journal | View Issue

Cite this: J. Mater. Chem. C, 2022, 10, 4590

Received 14th November 2021,
Accepted 24th January 2022

DOI: 10.1039/d1tc05487b

rsc.li/materials-c

A gold(III)–TADF emitter as a sensitizer for high-color-purity and efficient deep-blue solution-processed OLEDs†

Dongling Zhou,[a] Siping Wu,[a] Gang Cheng *[abc] and Chi-Ming Che *[abc]

Herein is described a blue-emitting gold(III)–TADF complex Au-1 that could act as a sensitizer for a solution-processed organic light-emitting diode (SP-OLED), in which a multi-resonance TADF emitter ν-DABNA is employed as the emissive dopant. Photophysical investigations revealed an efficient energy transfer (ET) process in the sensitized system with estimated Förster distance of 2.83 nm and ET rate of 2.35 × 10^7 s^{-1}. The fabricated blue SP-OLEDs attained high maximum external quantum efficiency of up to 16.6%, high color purity with a full-width at half maximum of 23 nm and Commission Internationale de L'Éclairage coordinates of (0.14, 0.18). A slight efficiency roll-off of 13% was observed for the Au-1 sensitized ν-DABNA-based device, which is much improved relative to that (30%) of the Au-1-based device, attributed to the effective ET process from Au-1 to ν-DABNA that could suppress the accumulation of triplet excitons on Au-1 at high luminance.

Introduction

Blue light-emitting materials are indispensable in the development of organic light-emitting diodes (OLEDs) for display and lighting applications.[1–4] However, compared to green and red ones, the development of blue-emitting materials simultaneously possessing high efficiency and color purity is lagging behind, particularly for low-cost solution-processed OLEDs (SP-OLEDs) that require emissive dopants to be highly soluble in common solvents.[5–16] Wang, Shao, and co-workers recently developed through-space charge transfer polymers containing face-to-face aligned donors and acceptors for achieving efficient blue thermally activated delayed fluorescence (TADF) emission.[6] The SP-OLEDs made with these polymers exhibited high maximum external quantum efficiency (EQE_{max}) of 18.8%. Nonetheless, the emission color was sky blue with Commission Internationale de LÉclairage (CIE) coordinates of (0.20, 0.31). Another blue SP-OLED employing a tris-triazolotriazine-based TADF emitter as an emissive dopant reported by Lee, Zhu, Wang, and co-workers gave EQE_{max} of 23.23% and sky-blue emission with CIE coordinates of (0.19, 0.36).[7] However, a severe efficiency roll-off of the device was observed with EQE at a luminance of 1000 cd m^{-2} (EQE_{1000}) of about 6%. Cho, Choi, and co-workers demonstrated three deep-blue to sky-blue TADF emitters bearing organoboron-based cores as acceptors and carbazole derivatives as donors.[9] A deep-blue SP-OLED made with one of these boron-based emitters showed EL at 424 nm with CIE coordinates of (0.17, 0.07), together with a narrow spectrum with a full-width at half maximum (FWHM) of 42 nm. Despite a decent EQE_{max} of 9.90% achieved for this device, the EQE_{1000} reduced to less than 1%. Continuous efforts have been devoted to this boron-based TADF system by the same group. These workers reported another ultra-deep-blue SP-OLED with improved EQE_{max} of 15.8% and CIE coordinates of (0.16, 0.05) relative to their previous results.[12]

Despite considerable efforts made to improve the performance of blue SP-OLEDs, the reported device performance data, particularly EQE and color purity, remain inferior to those of blue OLEDs manufactured using a vacuum deposition technique, especially for those with multi-resonance TADF compounds as emissive dopants.[17–25] In 2016, Hatakeyama and co-workers reported a rigid polycyclic framework consisting of nitrogen and boron atoms positioned oppositely and first proposed a concept of multi-resonance TADF.[19] Since then, many high-performance multi-resonance TADF emitters with extremely narrow emission bandwidths and relatively large oscillator strength of radiative transition have been developed. A solution-processable multi-resonance TADF material (OAB-ABP-1) with an extended π-skeleton and bulky substituents was designed and utilized in the fabrication of SP-OLEDs.[26] A high EQE_{max} of 21.8% and EQE_{1000} of 17.4% were achieved with the as fabricated pure green SP-OLEDs that showed CIE

[a] State Key Laboratory of Synthetic Chemistry, Department of Chemistry, The University of Hong Kong, Pokfulam Road, Hong Kong SAR, China. E-mail: ggcheng@hku.hk, cmche@hku.hk
[b] Hong Kong Quantum AI Lab Limited, 17 Science Park West Avenue, Pak Shek Kok, Hong Kong SAR
[c] HKU Shenzhen Institute of Research and Innovation, Shenzhen 518053, China

† Electronic supplementary information (ESI) available. See DOI: 10.1039/d1tc05487b

coordinates of (0.12, 0.63) and a narrow electroluminescent (EL) spectrum with a FWHM of 33 nm. Nonetheless, the examples of blue SP-OLEDs fabricated with multi-resonance TADF emitters are scarce,[15,27] and one of the related studies reported that the performance of SP-OLEDs was far inferior to that of vacuum-deposited OLEDs based on the same dopant probably attributable to the unsatisfactory film quality by the spin-coating method.[15] Multi-resonance TADF compounds usually show poor solubility as a result of their high molecular rigidity and planarity.

Phosphorescence- or TADF-sensitized fluorescence (PSF or TASF, depending on the emission mechanism of the sensitizer) is a cascade energy transfer (ET) process in which the excited state energy is transferred from the host to the fluorescent dopant *via* a phosphorescent or TADF sensitizer.[28–33] Such PSF/TASF OLEDs take advantage of both phosphorescence/TADF sensitizers and fluorescent emitters, exhibiting the high efficiency of phosphorescence/TADF, and the high color purity and long operational lifetime of fluorescence, and therefore are regarded as generation-3.5 OLEDs.[34] Recent studies demonstrated that multi-resonance TADF emitters could replace conventional fluorescent dopants to attain high-performance blue-emitting PSF/TASF OLEDs fabricated by vacuum deposition.[35–39] Enlightened by these recent advances, the obstacles of poor solubility of multi-resonance TADF emitters and inefficient ET from the hosts to multi-resonance TADF emitters, which hamper the development of blue SP-OLEDs, could be overcome by incorporating TADF sensitizers in the emitting layers (EMLs) to develop TASF devices.

In the present study, we demonstrated a deep-blue SP-OLED by utilizing a blue-emitting gold(III)–TADF complex **Au-1** as the sensitizer. This gold(III) complex showed a high emission quantum yield of 82% in a thin film and high-energy electroluminescence with λ_{max} at 470 nm.[8] A multi-resonance TADF emitter ν-DABNA was selected as a guest molecule as it was reported to show excellent performance in vacuum-deposited OLEDs in which a high EQE_{max} of 34.4%, deep blue electroluminescence with CIE coordinates of (0.12, 0.11) and narrowband emission (FWHM = 18 nm) were achieved.[20] To realize an efficient TASF OLED, effective ET from the host to **Au-1** and then to ν-DABNA are crucial. Efficient ET from the host 2,6-bis(9*H*-carbazol-9-yl)pyridine (PYD2) to **Au-1** has been observed in our previous work,[8] and the ET from **Au-1** to ν-DABNA is the subject of investigation in this work.

Results and discussion

Energy transfer from Au-1 to ν-DABNA

With an aim to investigate the ET process in the **Au-1**:ν-DABNA sensitized system, the absorption spectrum of ν-DABNA and emission spectrum of the sensitizer **Au-1** were measured. As portrayed in Fig. 1, there is a decent spectral overlap between the emission of **Au-1** and the absorption of ν-DABNA, suggesting that an effective ET from **Au-1** to ν-DABNA could occur. The ET process of the sensitized system was further examined in PYD2 thin films. After doping with ν-DABNA, the emission lifetimes of the **Au-1**:ν-DABNA sensitized system significantly decreased relative to that of **Au-1** only and there is no residual emission from the sensitizer **Au-1**, as shown in Fig. 2. These observations altogether suggest effective ET in this sensitized system upon photo-excitation.

Given the low dopant concentration of the guest emitter ν-DABNA (0.5 wt%), short-range Dexter ET can be ignored in which all guest molecules should be located adjacent to a host molecule, and Förster resonance energy transfer (FRET) is therefore considered as the dominant ET process in our sensitized system. The Förster distance (R_0) is commonly utilized to evaluate the efficiency of a FRET process and can be expressed by the following eqn (1):[40,41]

$$R_0^6 = \phi_D k^2 \left(\frac{9000(\ln 10)}{128\pi^5 N_A n^4}\right) \int_0^\infty F_D(\lambda)\varepsilon_A(\lambda)\lambda^4 d\lambda \qquad (1)$$

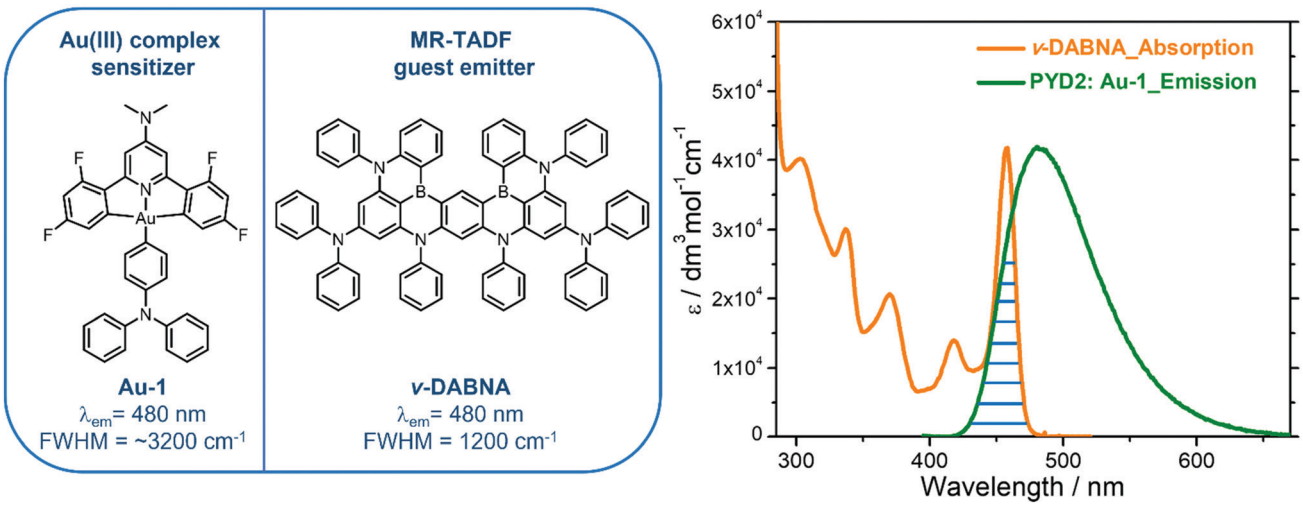

Fig. 1 Left: Chemical structures of **Au-1** and ν-DABNA (the given λ_{em} and FWHM measured in PYD2 films). Right: UV-Vis absorption spectrum of ν-DABNA in a toluene solution (2×10^{-5} mol dm^{-3}, rt) and normalized emission spectrum of **Au-1** doped in PYD2 thin films (10 wt%).

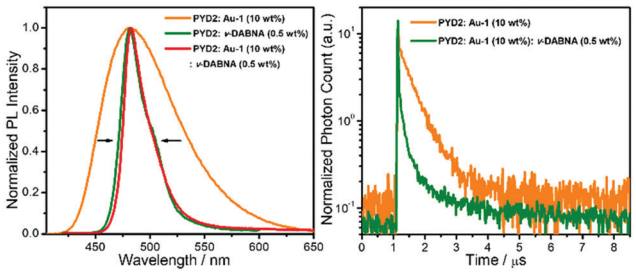

Fig. 2 Left: Normalized emission spectra of the corresponding thin films. Right: Emission decays for the corresponding thin films (λ_{em} = 480 nm). The weighted lifetimes are 0.52 μs for **Au-1** doped in PYD2 and 0.12 μs for the sensitized system.

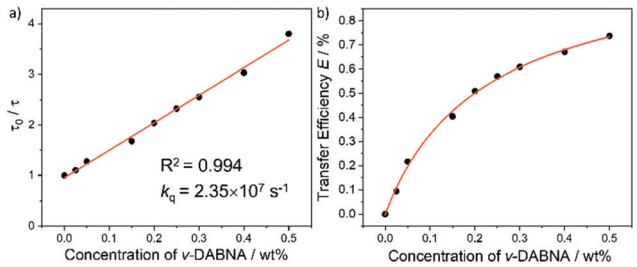

Fig. 3 (a) Stern–Volmer plot of the sensitized system PYD2:**Au-1** (10 wt%):ν-DABNA (0–0.5 wt%). The emission lifetimes were measured at 450 nm. The straight line is a linear fit to the data. (b) The plot of transfer efficiency *versus* the concentration of ν-DABNA.

where Φ_D is the emission quantum yield of the donor in the absence of the acceptor, and κ^2 is usually taken as 2/3, which is appropriate for dynamic random averaging of the donor and acceptor. n is the refractive index, whose value is 1.7 for most organic compounds. $F_D(\lambda)$ stands for the normalized emission spectrum of the donor. $\varepsilon_A(\lambda)$ and N_A are the molar absorptivity of the acceptor and the Avogadro's number, respectively. Based on the above formula, R_0 was calculated to be 2.81 nm, indicative of an effective FRET process between **Au-1** and ν-DABNA. The distance between the host and guest (R_{hg}) can be calculated based on the following formula (2):[40,41]

$$R_{hg} = \left(\frac{4\pi}{3} \times \beta \times \rho \times N_A \Big/ M_C\right)^{-\frac{1}{3}} \quad (2)$$

where β refers to the fraction of guest in the doping film, ρ stands for the density of the doping film, of which the value is usually taken as 1 g cm^{-3}. M_C is the molecular weight of the guest. The R_{hg} was estimated to be 1.92 nm for the sensitized system. The rate of ET (k_{ET}) and efficiency of FRET (E) from **Au-1** to ν-DABNA can be therefore calculated based on the following eqn (3) and (4):[40,41]

$$k_{ET} = \frac{1}{\tau_h}\left(\frac{R_0}{R_{hg}}\right)^6 \quad (3)$$

$$E = \frac{k_{ET}}{k_{ET} + \frac{1}{\tau_h}} = \frac{1}{1 + \left(\frac{R_{hg}}{R_0}\right)^6} \quad (4)$$

where τ_h stands for the emission lifetime of the donor in the absence of the acceptor. k_{ET} and E were calculated to be 1.89 × 10^7 s^{-1} and 91%, respectively. Emission quenching of **Au-1** resulting from the addition of ν-DABNA was observed and the quenching rate constant (k_q) should be related to the k_{ET}. In this regard, k_{ET} can be experimentally determined by the plot of the concentration of ν-DABNA *versus* τ_0/τ according to eqn (5):[42]

$$\frac{\tau_0}{\tau} = 1 + k_q\tau_0[Q] \quad (5)$$

where τ_0 is the emission lifetime of **Au-1** in the absence of ν-DABNA, τ is the emission lifetime of **Au-1** in the presence of ν-DABNA and [Q] is the concentration of ν-DABNA. For investigation of the ET rate, spin-coated films of the systems PYD2:**Au-1**(10 wt%):ν-DABNA(X wt%, X = 0, 0.025, 0.05, 0.15, 0.2, 0.25, 0.3, 0.4, and 0.5) were prepared. The decay of **Au-1** emission became faster with increasing concentration of ν-DABNA, together with a progressive decrease in the emission bandwidth (Fig. S4c, ESI†). This is because there are more energy acceptors of ν-DABNA present, which can quench the emission of **Au-1**. Fig. 3a presents a linear relationship between τ_0/τ and [Q], revealing that the Stern–Volmer relationship is obeyed. The prepared films were transparent and ν-DABNA molecules were assumed to be distributed homogeneously in the sensitized system. The k_q was estimated from the slope ($k_q\tau_0$) of the plot, being 2.35 × 10^7 s^{-1}, which is slightly faster than the theoretically calculated k_{ET} (1.89 × 10^7 s^{-1}). The estimated k_{ET} values are much faster than the radiative decay rate of **Au-1** (5.38 × 10^5 s^{-1}, Table S1, ESI†), suggestive of an efficient ET process. The relationship between energy transfer efficiency E and the concentration of ν-DABNA can be described by eqn (6).[43]

$$E = 1 - \frac{\tau}{\tau_0} \quad (6)$$

As portrayed in Fig. 3b, the transfer efficiency E reaches 50% at a concentration of 0.196 wt%. Assuming that this concentration corresponds to an average of one acceptor molecule in a sphere of radius R_0 and an average film density of 1 g cm^{-3}, R_0 was estimated to be 2.83 nm,[44] comparable to the value calculated based on eqn (1).

Film surface morphology

The film-forming ability and film morphology of solution-processed films prepared with PYD2:ν-DABNA(2 wt%), PYD2:**Au-1**(10 wt%):ν-DABNA(0.5 wt%) and PYD2:**Au-1** (10 wt%):ν-DABNA(2 wt%) were investigated by atomic force microscopy (AFM) in tapping mode. As observed from the AFM images in Fig. 4, the average roughness (R_a)/root mean square (RMS) roughness (R_q) values were found to be 5.953 nm/8.463 nm for the sample PYD2:ν-DABNA(2 wt%), 1.883 nm/2.345 nm for the sample PYD2:**Au-1**(10 wt%):ν-DABNA(0.5 wt%) and 3.148 nm/4.727 nm for the sample PYD2:**Au-1**(10 wt%):ν-DABNA(2 wt%), respectively. In comparison to the film made

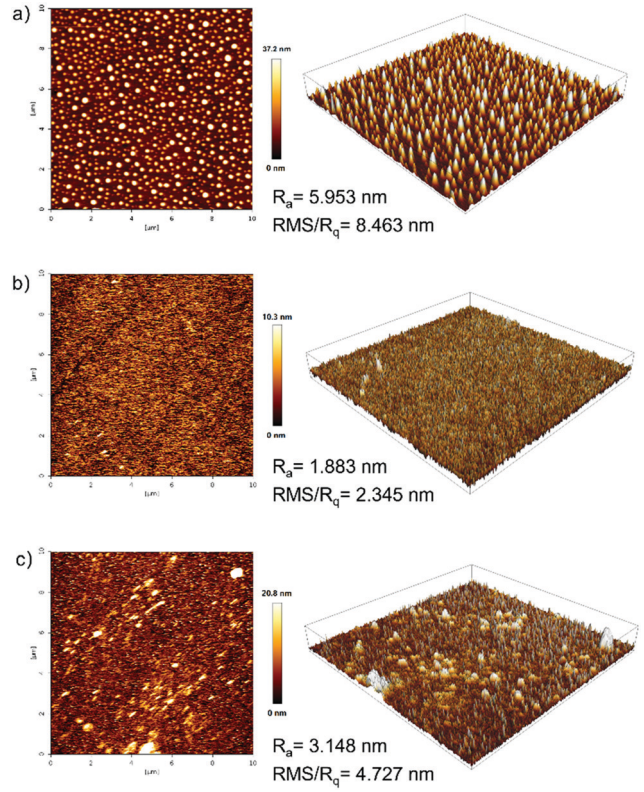

Fig. 4 2D and 3D AFM images (10 × 10 μm) with corresponding R_a and R_q values of three thin-film samples (a) PYD2:*ν*-DABNA (2 wt%), (b) PYD2:**Au-1**(10 wt%):*ν*-DABNA (0.5 wt%) and (c) PYD2:**Au-1**(10 wt%):*ν*-DABNA (2 wt%).

with only *ν*-DABNA (2 wt%), the sample of PYD2:**Au-1** (10 wt%):*ν*-DABNA(2 wt%) showed much smaller RMS value, suggestive of the improved film quality after incorporating **Au-1**. Apparently, the film made with PYD2:**Au-1**(10 wt%):*ν*-DABNA(0.5 wt%) displayed a smoother and more uniform profile than the sensitized system with 2 wt% *ν*-DABNA, having smaller R_a and RMS values, suggesting better film-forming capability.

This can be attributed to the good compatibility between PYD2, **Au-1** and *ν*-DABNA at their respective concentrations used. These results verify that our sensitized systems possess high compatibility and morphological stabilities, accounting for our promising solution-processed OLEDs based on the sensitized system under the optimized conditions used.

Device characteristics of blue-emitting SP-OLEDs

TASF SP-OLEDs were fabricated by adopting **Au-1** as a TADF sensitizer and *ν*-DABNA as a deep-blue emissive dopant. As shown in Fig. 5, the device architecture was ITO/PEDOT:PSS/PYD2:**Au-1**:*ν*-DABNA (50 nm)/DPEPO (10 nm)/TPBi (40 nm)/LiF (1.2 nm)/Al (100 nm), in which PYD2 was utilized as the host material in the EML. Bis[2-(diphenylphosphino)phenyl]ether oxide (DPEPO) and 1,3,5-tris(1-phenyl-1*H*-benzo[*d*]imidazol-2-yl)benzene (TPBi) function as hole/exciton blocking and electron transporting materials, respectively. **Au-1** and *ν*-DABNA

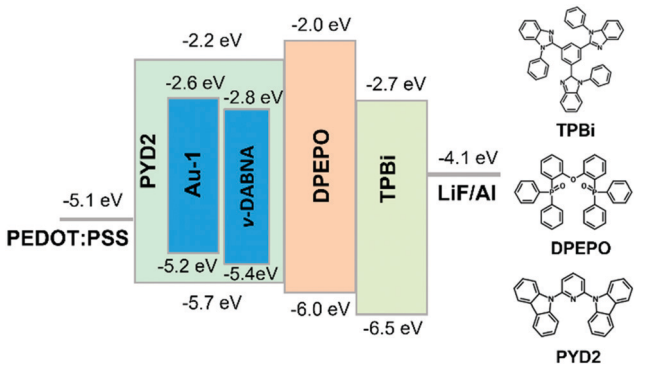

Fig. 5 Schematic device structure with proposed energy level diagrams and chemical structures of supportive organic materials.

were co-doped in the PYD2 host in the EML with different concentrations. As depicted in Fig. 6a, the EL spectrum of the device with 10 wt% **Au-1** and 0.5 wt% *ν*-DABNA is much narrower than that of the device with 10 wt% **Au-1** only and slightly broader than that of the device with 0.5 wt% *ν*-DABNA only, suggesting an efficient ET from **Au-1** to *ν*-DABNA. However, when compared with the corresponding emission spectra shown in Fig. 2 in which the emission of the **Au-1**:*ν*-DABNA sensitized system and *ν*-DABNA only are almost identical, the ET from **Au-1** to *ν*-DABNA shown in the EL spectrum is slightly incomplete, presumably due to the different excitation processes of electroluminescence and photoluminescence. In the photoluminescence measurements, PYD2 is first excited by light at a wavelength of 330 nm. It then transfers the excited state energy to *ν*-DABNA by a cascade ET *via* **Au-1**. On the other hand, in the TASF SP-OLED, direct charge trapping on both **Au-1** and *ν*-DABNA molecules may play a main role in exciton formation. Fig. 5 shows that both the LUMO and HOMO levels

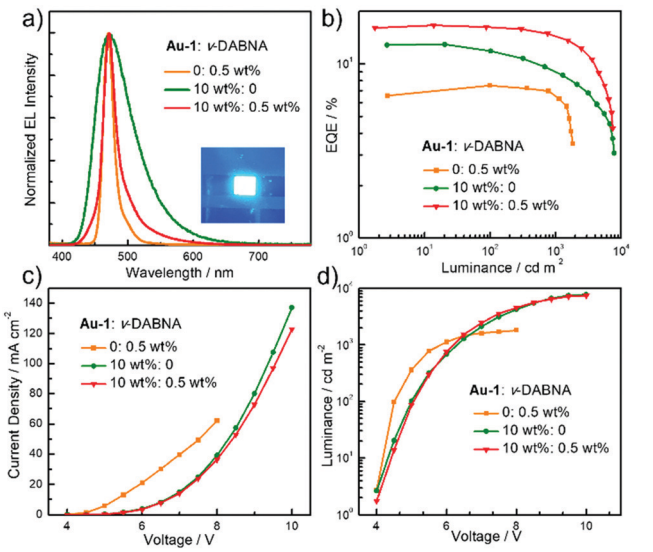

Fig. 6 (a) Normalized EL spectra, (b) EQE–luminance, (c) current density–voltage, and (d) luminance–voltage characteristics of SP-OLEDs with different concentrations of **Au-1** and *ν*-DABNA. The image of the sensitized SP-OLED is shown in the inset of (a).

of **Au-1** and *ν*-DABNA are within those of PYD2, suggesting the possibility of trapping both holes and electrons on **Au-1** and *ν*-DABNA molecules. The trapping effect is supported by the current density–voltage characteristics shown in Fig. 6c and Fig. S1c (ESI†), in which the current density decreased with increasing dopant concentration at a certain driving voltage. The trapping effect may influence the cascade ET, leading to a slightly incomplete ET from **Au-1** to *ν*-DABNA, as shown in Fig. 6a. When *ν*-DABNA was utilized as the emissive dopant alone, the EL spectrum with a narrow FWHM of 18 nm remained almost unchanged upon increasing the doping concentration of *ν*-DABNA from 0.5 to 2 wt% (Fig. S2a, ESI†). The EQE_{max} of the *ν*-DABNA-based device was 7.51% at a low dopant concentration of 0.5 wt%, increased to 8.60% at a higher concentration of 1 wt% and then decreased to 7.30% at an even higher concentration of 2 wt%. The relatively lower EQE_{max} at a low concentration of 0.5 wt% might be due to incomplete ET from the host PYD2, whose emission can be observed in the enlarged EL spectrum shown in Fig. S2c (ESI†). A decrease in the EQE_{max} of the device at a higher concentration of *ν*-DABNA (2 wt%) might be attributable to concentration quenching.[17] As depicted in Fig. S1a (ESI†), the EL spectra became narrower with increasing concentration ratios of *ν*-DABNA to **Au-1** in the sensitized devices because of the trapping effects of both *ν*-DABNA and **Au-1**. In the device with a higher concentration ratio of *ν*-DABNA to **Au-1**, more excitons directly formed on the *ν*-DABNA molecules. Since the EL spectrum of the sensitized device is the combined emission from both *ν*-DABNA and **Au-1**, more exciton formation and recombination on *ν*-DABNA would cause more *ν*-DABNA portion in the observed EL emission, resulting in a narrower EL spectrum. As depicted in Fig. 6b and Fig. S1b (ESI†), the TASF OLED with 10 wt% **Au-1** and 0.5 wt% *ν*-DABNA showed an EQE_{max} as high as 16.6%. Although direct charge trapping is the primary mechanism of exciton formation in the TASF devices, the efficient ET from **Au-1** to *ν*-DABNA resulted in an extremely narrow EL spectrum with a FWHM of 23 nm and CIE coordinates of (0.14, 0.18) in the sensitized device made with 0.5 wt% *ν*-DABNA and 10 wt% **Au-1** (Fig. 6a). Therefore, different from the incomplete ET from the host PYD2 to *ν*-DABNA in the *ν*-DABNA-based device with a low dopant concentration of 0.5% (Fig. S2, ESI†), by cascade ET, all excitons formed on the host PYD2 were transferred to *ν*-DABNA *via* **Au-1** in the TASF device, leading to a highly improved EQE_{max}. The EQE_{max} of the sensitized device (16.6%) is higher than that of the **Au-1**-based device (12.9%), probably because the sensitized system is capable of recycling the triplet excitons quenched by the host.[38] In addition, the efficient FRET process of the sensitized system could suppress the accumulation of triplet excitons on the sensitizer, leading to alleviated efficiency roll-offs. As shown in Fig. 6b, an EQE_{1000} of 14.4% was achieved in the best-sensitized device, corresponding to an efficiency roll-off of 13%, which is much improved relative to that (30%) of the **Au-1**-based device. With the increased concentration of *ν*-DABNA, the EQE_{max} of the sensitized devices decreased (Table S2, ESI†). This might be due to the concentration quenching of *ν*-DABNA. Additionally, in comparison to the sensitized system of PYD2:**Au-1**(10 wt%):*ν*-DABNA(0.5 wt%), the system of PYD2:**Au-1**(10 wt%):*ν*-DABNA(2 wt%) showed poor film-forming ability, as aforementioned, together resulting in a lower EQE_{max}. The efficiency of the TASF device with 10 wt% **Au-1** and 0.5 wt% *ν*-DABNA is among the best of the reported blue-emitting SP-OLEDs, particularly those with CIE_y less than 0.2, as shown in Fig. 7.[5,9,11,12,14,15] The preliminary lifetime of the device with 10 wt% **Au-1** and 0.5 wt% *ν*-DABNA was measured under our laboratory conditions. As shown in Fig. S3 (ESI†), the operational lifetime at 50% of the initial luminance of 1000 cd m^{-2} (LT_{50}) was 16 min. Similar results have been reported for blue SP-OLEDs with similar device structures,[7,10] and the relatively short lifetime could be attributed to a lack of device optimization and the harmful effect of PEDOT:PSS.

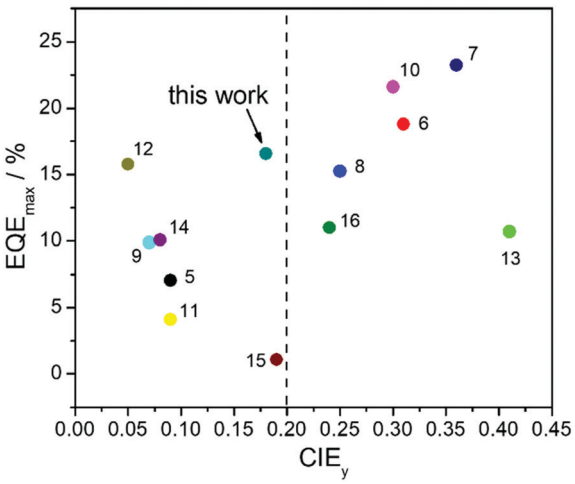

Fig. 7 Summary of EQE_{max} and CIE_y values of recently reported SP-OLEDs. The reference numbers are presented next to the relevant data points.

Conclusions

In summary, a high EQE_{max} of 16.6%, high color purity with a FWHM of 23 nm and CIE coordinates of (0.14, 0.18) were simultaneously actualized in an optimized TASF SP-OLED by employing **Au-1** as a TADF sensitizer and *ν*-DABNA as a deep-blue emitter. Owing to the efficient cascade ET from PYD2 to *ν*-DABNA *via* **Au-1** and the recycling of triplet excitons that were wasted in the **Au-1**-based TADF devices of the TASF system, the EQE_{max} of the TASF device was found to be higher than those of both the **Au-1**- and *ν*-DABNA-based ones. A severe efficiency roll-off of 30% was found for the **Au-1**-based device because of accumulation of triplet excitons on **Au-1** at high brightness. By incorporating 0.5 wt% *ν*-DABNA, the efficiency roll-offs in the sensitized device were significantly reduced down to 13%, attributable to the suppressed accumulation of triplet excitons on **Au-1** at high luminance due to efficient ET in the TASF device.

Experimental section

Materials

PYD2, DPEPO, TPBi, *ν*-DABNA and LiF were purchased from Luminescence Technology Corp; PEDOT: PSS was purchased from Heraeus. All of these materials were used as received. **Au-1** was synthesized based on the reported method.[8]

Measurements

The procedure for the preparation of thin-film samples for kinetic studies is described as follows: the mixture of PYD2 and dopant(s) in chlorobenzene (10 mg mL^{-1}) was spin coated on quartz films at a speed of 500 rpm inside a glove box and transparent film samples were obtained after being annealed at 70 °C for 20 minutes. The emission lifetimes were recorded at 450 nm and the data points after the prompt fluorescence signal stemming from *ν*-DABNA were considered to be the emission decay of **Au-1** and fitted by using the equation of $y = y_0 + Ae^{-\frac{x}{t}}$. The procedure for the preparation of thin-film samples for AFM measurement is described as follows: the mixture of PYD2 and dopant(s) in chlorobenzene (10 mg mL^{-1}) was spin coated on quartz slides at a speed of 3000 rpm inside a glove box and the transparent thin films were obtained after being annealed at 70 °C for 20 minutes. The prepared films were examined by atomic force microscopy (AFM) in tapping mode (a Bruker Nano Wizard ULTRA Speed 2 instrument). Emission quantum yields of these thin-film samples were measured using a Hamamatsu C11347 Quantaurus-QY Absolute PL quantum yields measurement system. The emission lifetime measurements were performed on an LP920-KS Laser Flash Photolysis spectrophotometer (Edinburgh Instrument Ltd) equipped with a Q-switched Nd:YAG laser. Emission spectra of these thin-film samples were recorded on a Horiba Fluorolog-3 spectrophotometer.

Device fabrication and characterization

An aqueous solution of PEDOT:PSS was spin-coated onto a cleaned ITO coated glass substrate and baked at 120 °C for 20 minutes to remove the residual water solvent inside a clean room. The mixture of PYD2 and emitting dopant(s) in chlorobenzene was spin-coated atop the PEDOT:PSS layer inside a glove box. After being annealed at 70 °C for 30 minutes, all devices were subsequently transferred into a Kurt J. Lesker SPECTROS vacuum deposition system without exposure to air. In the vacuum chamber, organic materials of DPEPO and TPBi were thermally deposited in sequence at a rate of ~0.1 nm s^{-1}. Finally, LiF (1.2 nm) and Al (100 nm) were thermally deposited at rates of 0.03 and 0.2 nm s^{-1}, respectively.

EL spectra, CIE coordinates, luminance-current–voltage characteristics, current efficiency, power efficiency, and EQE were measured using a Keithley 2400 source-meter and an absolute external quantum efficiency measurement system (C9920-12, Hamamatsu Photonics). All devices were characterized at room temperature under an ambient air environment without encapsulation. The operational lifetimes of the devices were measured in a glove box with both concentrations of O_2 and H_2O lower than 1 ppm. The efficiency roll-offs were evaluated based on the formula of $[(EQE_{max} - EQE_{1000})/EQE_{max}] \times 100$ in which the EQE_{max} and EQE_{1000} refer to maximum EQE and EQE at a luminance of 1000 cd m^{-2}, respectively.

Conflicts of interest

There are no conflicts of interest to declare.

Acknowledgements

This research was funded by the Major Program of Guangdong Basic and Applied Research (2019B030302009), the Basic Research Program of Shenzhen (JCYJ20170818141858021 and JCYJ20200109150414471), Shunde Science and Technology Bureau (2030218000158), Innovation and Technology Fund (PRP/071/19/FX) and Hong Kong Quantum AI Lab Limited.

References

1 Y. Im, S. Y. Byun, J. H. Kim, D. R. Lee, C. S. Oh, K. S. Yook and J. Y. Lee, *Adv. Funct. Mater.*, 2017, **27**, 1603007.
2 J.-H. Lee, C.-H. Chen, P.-H. Lee, H.-Y. Lin, M.-K. Leung, T.-L. Chiu and C.-F. Lin, *J. Mater. Chem. C*, 2019, **7**, 5874–5888.
3 Z. Xu, B. Z. Tang, Y. Wang and D. Ma, *J. Mater. Chem. C*, 2020, **8**, 2614–2642.
4 M.-C. Tang, M.-Y. Chan and V. W.-W. Yam, *Chem. Rev.*, 2021, **121**, 7249–7279.
5 H. Usta, D. Alimli, R. Ozdemir, S. Dabak, Y. Zorlu, F. Alkan, E. Tekin and A. Can, *ACS Appl. Mater. Interfaces*, 2019, **11**, 44474–44486.
6 Q. Li, J. Hu, J. Lv, X. Wang, S. Shao, L. Wang, X. Jing and F. Wang, *Angew. Chem., Int. Ed.*, 2020, **59**, 20174–20182.
7 X. Chen, S. Wang, H. L. Lee, J. Y. Lee, X. Liao, L. Li, W. Zhu and Y. Wang, *Adv. Opt. Mater.*, 2021, **9**, 2101518.
8 D. Zhou, G. Cheng, G. S. M. Tong and C.-M. Che, *Chem. – Eur. J.*, 2020, **26**, 15718–15726.
9 H. J. Kim, M. Godumala, S. K. Kim, J. Yoon, C. Y. Kim, H. Park, J. H. Kwon, M. J. Cho and D. H. Choi, *Adv. Opt. Mater.*, 2020, **8**, 1902175.
10 G. Kreiza, D. Berenis, D. Banevičius, S. Juršėnas, T. Javorskis, E. Orentas and K. Kazlauskas, *Chem. Eng. J.*, 2021, **412**, 128574.
11 P. Therdkatanyuphong, C. Kaiyasuan, P. Chasing, T. Kaewpuang, T. Chawanpunyawat, T. Sudyoadsuk and V. Promarak, *ACS Appl. Electron. Mater.*, 2021, **3**, 1311–1322.
12 H. J. Kim, H. Kang, J.-E. Jeong, S. H. Park, C. W. Koh, C. W. Kim, H. Y. Woo, M. J. Cho, S. Park and D. H. Choi, *Adv. Funct. Mater.*, 2021, **31**, 2102588.
13 J. Hwang, C. Y. Kim, H. Kang, J.-E. Jeong, H. Y. Woo, M. J. Cho, S. Park and D. H. Choi, *J. Mater. Chem. C*, 2020, **8**, 16048–16056.

14 J. Hwang, H. Kang, J.-E. Jeong, H. Y. Woo, M. J. Cho, S. Park and D. H. Choi, *Chem. Eng. J.*, 2021, **416**, 129185.
15 T. Xu, X. Liang and G. Xie, *Front. Chem.*, 2021, **9**, 691172.
16 Y. Chen, N. Li, Z. Huang, G. Xie and C. Yang, *Chem. Eng. J.*, 2022, **430**, 133078.
17 S. M. Suresh, D. Hall, D. Beljonne, Y. Olivier and E. Zysman-Colman, *Adv. Funct. Mater.*, 2020, **30**, 1908677.
18 J.-M. Teng, Y.-F. Wang and C.-F. Chen, *J. Mater. Chem. C*, 2020, **8**, 11340–11353.
19 T. Hatakeyama, K. Shiren, K. Nakajima, S. Nomura, S. Nakatsuka, K. Kinoshita, J. Ni, Y. Ono and T. Ikuta, *Adv. Mater.*, 2016, **28**, 2777–2781.
20 Y. Kondo, K. Yoshiura, S. Kitera, H. Nishi, S. Oda, H. Gotoh, Y. Sasada, M. Yanai and T. Hatakeyama, *Nat. Photonics*, 2019, **13**, 678–682.
21 D. Hall, S. M. Suresh, P. L. dos Santos, E. Duda, S. Bagnich, A. Pershin, P. Rajamalli, D. B. Cordes, A. M. Z. Slawin, D. Beljonne, A. Köhler, I. D. W. Samuel, Y. Olivier and E. Zysman-Colman, *Adv. Opt. Mater.*, 2020, **8**, 1901627.
22 M. Yang, I. S. Park and T. Yasuda, *J. Am. Chem. Soc.*, 2020, **142**, 19468–19472.
23 S. Oda, W. Kumano, T. Hama, R. Kawasumi, K. Yoshiura and T. Hatakeyama, *Angew. Chem., Int. Ed.*, 2021, **60**, 2882–2886.
24 J. Wei, C. Zhang, D. Zhang, Y. Zhang, Z. Liu, Z. Li, G. Yu and L. Duan, *Angew. Chem., Int. Ed.*, 2021, **60**, 12269–12273.
25 M. Nagata, H. Min, E. Watanabe, H. Fukumoto, Y. Mizuhata, N. Tokitoh, T. Agou and T. Yasuda, *Angew. Chem., Int. Ed.*, 2021, **60**, 20280–20285.
26 N. Ikeda, S. Oda, R. Matsumoto, M. Yoshioka, D. Fukushima, K. Yoshiura, N. Yasuda and T. Hatakeyama, *Adv. Mater.*, 2020, **32**, 2004072.
27 S. Xu, Q. Yang, Y. Zhang, H. Li, Q. Xue, G. Xie, M. Gu, J. Jin, L. Huang and R. Chen, *Chin. Chem. Lett.*, 2021, **32**, 1372–1376.
28 M. A. Baldo, M. E. Thompson and S. R. Forrest, *Nature*, 2000, **403**, 750–753.
29 H. Nakanotani, T. Higuchi, T. Furukawa, K. Masui, K. Morimoto, M. Numata, H. Tanaka, Y. Sagara, T. Yasuda and C. Adachi, *Nat. Commun.*, 2014, **5**, 4016.
30 P.-K. Chow, G. Cheng, G. S. M. Tong, C. Ma, W.-M. Kwok, W.-H. Ang, C. Y.-S. Chung, C. Yang, F. Wang and C.-M. Che, *Chem. Sci.*, 2016, **7**, 6083–6098.
31 S. Y. Byeon, D. R. Lee, K. S. Yook and J. Y. Lee, *Adv. Mater.*, 2019, **31**, 1803714.
32 D. Zhang, X. Song, M. Cai and L. Duan, *Adv. Mater.*, 2018, **30**, 1705250.
33 X. Song, D. Zhang, Y. Lu, C. Yin and L. Duan, *Adv. Mater.*, 2019, **31**, 1901923.
34 X.-K. Chen, D. Kim and J.-L. Brédas, *Acc. Chem. Res.*, 2018, **51**, 2215–2224.
35 D. Zhang, X. Song, A. J. Gillett, B. H. Drummond, S. T. E. Jones, G. Li, H. He, M. Cai, D. Credgington and L. Duan, *Adv. Mater.*, 2020, **32**, 1908355.
36 W. J. Chung, K. H. Lee, M. Jung, K. M. Lee, H. C. Park, M.-S. Eum and J. Y. Lee, *Adv. Opt. Mater.*, 2021, **9**, 2100203.
37 S. Nam, J. W. Kim, H. J. Bae, Y. M. Maruyama, D. Jeong, J. Kim, J. S. Kim, W.-J. Son, H. Jeong, J. Lee, S.-G. Ihn and H. Choi, *Adv. Sci.*, 2021, **8**, 2100586.
38 S. O. Jeon, K. H. Lee, J. S. Kim, S.-G. Ihn, Y. S. Chung, J. W. Kim, H. Lee, S. Kim, H. Choi and J. Y. Lee, *Nat. Photonics*, 2021, **15**, 208–215.
39 C.-Y. Chan, M. Tanaka, Y.-T. Lee, Y.-W. Wong, H. Nakanotani, T. Hatakeyama and C. Adachi, *Nat. Photonics*, 2021, **15**, 203–207.
40 C. Zhang, Y. Lu, Z. Liu, Y. Zhang, X. Wang, D. Zhang and L. Duan, *Adv. Mater.*, 2020, **32**, 2004040.
41 J. Zeng, J. Guo, H. Liu, Z. Zhao and B. Z. Tang, *Adv. Funct. Mater.*, 2020, **30**, 2000019.
42 F. Laquai, Y.-S. Park, J.-J. Kim and T. Basché, *Macromol. Rapid Commun.*, 2009, **30**, 1203–1231.
43 B. Stender, S. F. Völker, C. Lambert and J. Pflaum, *Adv. Mater.*, 2013, **25**, 2943–2947.
44 T. Förster, *Discuss. Faraday Soc.*, 1959, **27**, 7–17.

